IEEE Access
Multidisciplinary | Rapid Review | Open Access Journal

Received January 12, 2021, accepted January 24, 2021, date of publication January 27, 2021, date of current version February 3, 2021.

Digital Object Identifier 10.1109/ACCESS.2021.3054837

Active Roll Stabilization With Disturbance Feedforward Control

SEONGJIN YIM, (Member, IEEE)
Research Center for Electrical and Information Technology, Seoul National University of Science and Technology, Seoul 01811, Republic of Korea
e-mail: acebtif@seoultech.ac.kr

This work was supported by the Seoul National University of Science and Technology through the Research Program.

ABSTRACT This article presents a method to design a controller for active roll stabilization (ARS) with a disturbance feedforward control. To design the controller, a linear 1-DOF roll model is adopted. With the model, three feedback controllers, i.e., linear quadratic regulator (LQR), H_∞ and sliding mode controller (SMC), are designed. Feedforward controller with the lateral acceleration is designed with a discrete-time state-space equation to improve roll control performance. To estimate the roll angle and the lateral acceleration simultaneously with noisy roll rate measurement, a discrete-time Kalman filter (DTKF) is used. When applying DTKF for state and disturbance estimation, a recursive least square (RLS) is adopted to estimate the parameters of 1-DOF roll model. As an actuator for ARS, an active anti-roll bar (AARB) and a continuous damping control (CDC) are adopted. To verify the performance of the proposed controllers, simulation is conducted on the vehicle simulation package, CarSim®. From simulation, it was verified that the proposed controllers can enhance the performance of active roll stabilization and that the effectiveness of CDC was investigated.

INDEX TERMS Active roll stabilization (ARS), disturbance feedforward control, discrete-time Kalman filter (DTKF), recursive least square (RLS), active anti-roll bar (AARB), continuous damping control (CDC).

I. INTRODUCTION

In vehicle control systems, an active roll stabilization (ARS) is a controller which tries to improve ride comfort and to prevent vehicle rollover by controlling the roll motion created by lateral acceleration [1]. There are several performance measures with respect to roll motion such as ride comfort, road adhesion, energy consumption, rattle space limitation and rollover prevention. Among them, the most important measure in applying ARS is the ride comfort [2]. Generally, the ride comfort for vertical motion is evaluated by vertical acceleration. For roll and pitch motions, it is evaluated by roll angle and pitch angle, respectively. Therefore, ARS for ride comfort aims to reduce the roll angle.

In general, vertical motion of a sprung mass has a high natural frequency around 10Hz, whereas roll motion has low natural one around 1Hz [2], [3]. So, a high-bandwidth actuator is not required as an actuator for ARS. An active suspension, an active anti-roll bar (AARB) and a continuous damping control (CDC) have been adopted as an actuator for ARS. Active suspension and CDC can control vertical, roll and pitch motions, but AARB can only control roll motion. When installing these devices on a real vehicle, the active suspension should be installed on four suspensions, but AARB only needs to be installed on the front and rear axles. Therefore, in terms of ARS, an AARB is more advantageous than an active suspension from a cost or energy consumption perspective. To date, various types of AARBs have been developed and have already been commercialized by Toyota and BMW [4], [5]. Different from active suspension or AARB, CDC is a semi-active device, which can generate a force to resist the suspension travel. Notable feature of CDC is a wider range of operating frequency, compared to active suspension. It has been known that CDC can cover the frequency range from 0 to 40Hz, whereas active suspension can do the frequency range from 0 to 30Hz. Moreover, CDC requires a smaller amount of energy than active suspension [6], [7]. However, the number of papers for ARS with CDC is relatively smaller than that of ARS with AARB although CDC has several benefits over AARB or active

The associate editor coordinating the review of this manuscript and approving it for publication was Shihong Ding.

suspension [8]–[10]. For the reasons, an AARB and a CDC are used as an actuator for ARS in this article. Especially, the motivation of this article is to check the performance of CDC for ARS.

To date, various control methods for ARS have been proposed [4], [8]–[15]. All of these methods adopted feedback control, and their performance is limited. In general, lateral acceleration can be easily obtained by using a sensor mounted on a vehicle. If a feedforward controller is designed and applied using the lateral acceleration signal, better control performance than the conventional feedback controller can be achieved [16]–[18]. In the previous works, the lateral acceleration as a disturbance was previewed with V2V communication. In this article, LQR, H_∞ and SMC are designed as a feedback controller for ARS in the discrete-time domain [16], [18]. In addition, the feedforward controller with the lateral acceleration signal is derived from the discrete-time state-space equation. In order to enhance the control performance of ARS, all the feedback controllers are combined with the feedforward controller [19].

Most of the controllers for ARS proposed so far require roll angle and roll rate information. Currently, the price of sensors used to measure roll angular velocity or roll rate is not very high [20], [21]. However, a sensor to measure the roll angle is quite expensive because it has built-in IMU (Inertial Measurement Unit) and Kalman filter [22]. Therefore, the roll angle should be estimated using an observer with measured roll rate signal. Recently, several studies have been conducted to estimate the roll and pitch angles using a low-cost IMU [23], [24]. Following the previous works, a discrete-time Kalman filter (DTKF) is adopted to estimate the roll angle from measured roll rate signal [25].

The feedforward controller proposed in this article needs lateral acceleration signal. However, signals measured from lateral acceleration sensor currently installed on the vehicle contains a lot of noise. Fig. 1 is the lateral acceleration and the roll rate signals measured using the accelerometer and the inertial measurement unit (IMU) installed on a real vehicle during the dual lane change steering at a speed of 60 km/h, respectively [22], [25]. If these signals are used for control, the noise components in the signals are directly passed to the control input, which can generate severe chattering in roll responses. So, it is necessary to apply a low-pass filter (LPF) to remove the sensor noise. However, a time delay occurs as a result of application of LPF. Moreover, two LPFs are needed to filter the noises in the lateral acceleration and roll rate signals. On the other hand, an observer, needed to estimate the roll angle in ARS, can play a role of LPF. So, it is desirable to design an observer which can estimate the roll angle and the lateral acceleration simultaneously with measured roll rate signal [19], [26]. In this article, the lateral acceleration is estimated using the observer with roll rate signal, and it is used for a feedforward control, not the lateral acceleration signal measured by a sensor [19], [27]. In the previous work, the lateral acceleration was estimated from roll rate measurement with DTKF [19]. Following the previous work, a DTKF is

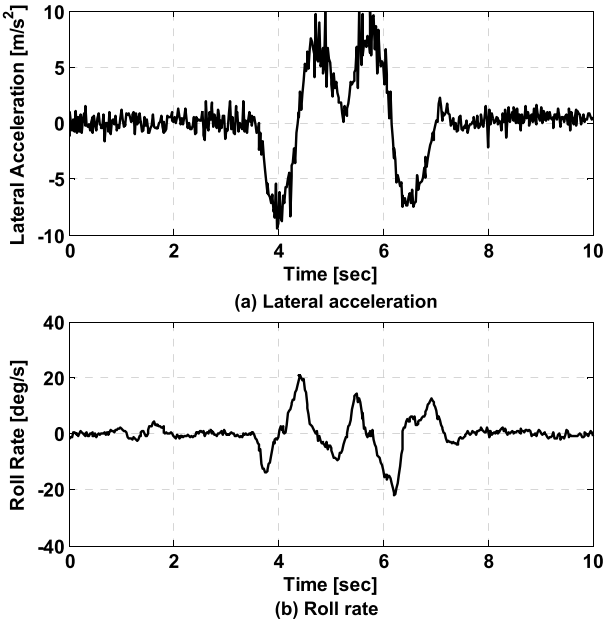

FIGURE 1. Lateral acceleration and roll rate signals measured from on-board accelerometer and inertial measurement unit on a real vehicle.

adopted to estimate the roll angle and the lateral acceleration simultaneously from the measured roll rate signal [27]. The roll angle and lateral acceleration information obtained using DTKF are used for feedback and feedforward controllers in ARS, respectively. So, the controllers used for ARS in this article are the observer-based controller. In summary, the second motivation of this article is to design a DTKF for estimating the roll angle and the lateral acceleration simultaneously instead of applying LPFs needed to filter the measured roll rate and lateral acceleration signals.

Generally, parameters in real vehicles vary according to driving conditions. So, it is necessary to estimate parameters of a vehicle model for better state estimation. For the purpose, uncertain or time-varying parameters have been estimated by parameter estimators such as least-mean-square (LMS) and recursive-least-square (RLS) algorithms [28]–[31]. For ARS, RLS was adopted to estimate the height of center of gravity [28]. Roll dynamics was identified with RLS for sliding mode state observer [29]. It has been known that an extended Kalman filter (EKF) is equivalent to RLS. Following the idea, the parameters of a roll model were estimated with dual EKFs [25]. RLS is simple to design and easy to implement. So, RLS is adopted as a parameter estimator in this article. The third motivation of this article is to check the effects of the parameter estimator, i.e., RLS, for the observer-based controller.

The controllers for ARS designed in this article consist of the feedback and feedforward controllers. The feedback controller uses the roll angle and the roll rate signals, and the feedforward controller uses the lateral acceleration signal. The roll angle and lateral acceleration signals are estimated with DTKF. So, this is a disturbance observer.

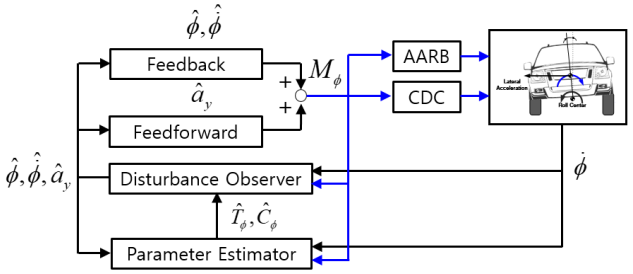

FIGURE 2. Schematic diagram of observer-based controller with state observer and parameter estimators for ARS.

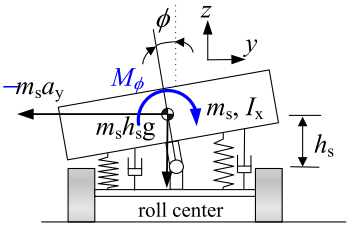

FIGURE 3. 1-DOF roll model.

When estimating these variables, parameters of a model is estimated with RLS. The schematic diagram of observer-based controller with state observer and parameter estimator for ARS is shown in Fig. 2.

The contributions of this article can be summarized as three points of view. The first is to design a feedforward controller from the discrete-time state-space model and to combine it with feedback controllers. The second is to design the disturbance observer for estimation and filtering purposes. Instead of using noisy measured lateral acceleration, it is estimated with DTKF and used for the feedforward controller. Moreover, RLS is applied with DTKF to estimate parameters of a model. The effect of RLS on the disturbance observer and on the performance of ARS is checked. The third is to check the effectiveness of the semi-active actuator, i.e., CDC, for ARS over the active one, i.e., AARB.

The structure of this article is as follows. In Section II, we construct a vehicle model and design LQR, H_∞ controller and SMC for ARS. The feedforward controller is also derived in this section. In Section III, we design an observer to estimate the roll angle and lateral acceleration and a RLS to estimate parameters of a vehicle model. In Section IV, simulation is performed to verify the designed controllers. Section V concludes this article.

II. CONTROLLER DESIGN FOR ARS

A. VEHICLE MODEL

In this article, the 1-DOF roll model, as shown in Fig. 3, is used for controller design [15]–[19]. A 4-DOF roll plane model can be used for controller design [14]. However, there are little differences in control performance between 1-DOF and 4-DOF models. So, 1-DOF roll model is used for controller design. The equation of motion of 1-DOF roll model is given as (1). As shown in (1), the roll motion is caused by the lateral acceleration a_y. Another source of the roll motion is a rode profile, which is not considered in this article. Eq. (2) shows the definition of the lateral acceleration that generates the roll motion. In (2), v_x, v_y, and γ are the longitudinal and lateral velocities, and the yaw rate, respectively. So, the primary source of the roll motion is the yaw rate, generated by steering of a driver. In (1), I_x, C_φ, K_φ, m_s and h_s are the roll moment of inertia, the roll damping coefficient, the roll stiffness, the sprung mass and the height of center of gravity from roll center, respectively.

$$I_x\ddot{\phi}(t) + C_\phi\dot{\phi}(t) + K_\phi\phi(t) - m_s h_s a_y(t) - m_s g h_s \phi(t) = M_\phi(t) \tag{1}$$

$$a_y(t) = \dot{v}_y(t) + v_x(t)\,\gamma(t) \tag{2}$$

In (1), the state variables in the model are the roll angle φ and the roll rate $\dot{\phi}$. If the state vector $\mathbf{x}$ is defined with the state variables as given in (3), the continuous-time state-space equation is obtained as (4) from (1) and (3). In (4), $\mathbf{w}$ is the lateral acceleration a_y as a disturbance, and $\mathbf{u}$ is the control roll moment M_φ as a control input.

$$\mathbf{x}(t) = \begin{bmatrix} \phi(t) & \dot{\phi}(t) \end{bmatrix}^T \tag{3}$$

$$\begin{cases} \dot{\mathbf{x}}(t) = \mathbf{A}\mathbf{x}(t) + \mathbf{B}_1\mathbf{w}(t) + \mathbf{B}_2\mathbf{u}(t) \\ \mathbf{A} = \begin{bmatrix} 0 & 1 \\ -\dfrac{K_\phi - m_s g h_s}{I_x} & -\dfrac{C_\phi}{I_x} \end{bmatrix}, \mathbf{B}_1 = \begin{bmatrix} 0 \\ \dfrac{m_s h_s}{I_x} \end{bmatrix}, \\ \mathbf{B}_2 = \begin{bmatrix} 0 \\ \dfrac{1}{I_x} \end{bmatrix} \end{cases} \tag{4}$$

By discretizing the continuous-time state-space equation, (4), over the sampling time T_s, the discrete-time state-space equation is obtained as (5). In (5), the definitions of the system matrices, Φ, Π and Γ, are given in (6). As shown in (6), the system matrices in (5) can be easily updated according to the change of parameters in (4).

$$\mathbf{x}(k+1) = \mathbf{\Phi}\mathbf{x}(k) + \mathbf{\Pi}\mathbf{w}(k) + \mathbf{\Gamma}\mathbf{u}(k) \tag{5}$$

$$\mathbf{\Phi} \cong \mathbf{I} + T_s \cdot \mathbf{A}e^{\mathbf{A}\tau}, \quad \mathbf{\Pi} \cong T_s \cdot \mathbf{B}_1, \quad \mathbf{\Gamma} \cong T_s \cdot \mathbf{B}_2 \tag{6}$$

B. DESIGN OF A CONTROLLER FOR ARS

In this article, three feedback controllers, LQR, H_∞ and SMC, are designed, and then a feedforward controller is derived from the discrete-time state-space equation.

First, a discrete-time LQR is designed using the discrete-time state-space equation, (5). The LQ objective function for ARS is given in (7) [16]–[18]. In (7), q_i is a weight for an individual term and is calculated as $q_i = (1/\rho_i)^2$ by Bryson's rule, where ρ_i is the maximum allowable value for each term. Eq. (7) is converted to (8) with the definitions of matrices given in (9). With the state-space equation of (5) and the LQ

objective function of (8), a LQR in the form of (10) is obtained by solving a Riccati equation.

$$J = \sum_{k=0}^{\infty} \left[q_1 \phi^2 (k) + q_2 \dot{\phi}^2 (k) + q_3 M_\phi^2 (k) \right] \tag{7}$$

$$\begin{aligned} J &= \sum_{k=0}^{\infty} \mathbf{z}^T (k)\, \mathbf{z} (k) \\ &= \sum_{k=0}^{\infty} \left[\mathbf{x}^T (k)\, \mathbf{Q}\mathbf{x} (k) + \mathbf{u} (k)\, \mathbf{R}\mathbf{u} (k) \right] \end{aligned} \tag{8}$$

$$\begin{cases} \mathbf{z} (k) \equiv \mathbf{C}\mathbf{x} (k) + \mathbf{D}\mathbf{u} (k), \ \mathbf{Q} \equiv \mathbf{C}^T \mathbf{C}, \\ \quad \mathbf{R} \equiv \mathbf{D}^T \mathbf{D} \\ \mathbf{C} \equiv \begin{bmatrix} \sqrt{q_1} & 0 \\ 0 & \sqrt{q_2} \\ 0 & 0 \end{bmatrix}, \mathbf{D} \equiv \begin{bmatrix} 0 \\ 0 \\ \sqrt{q_3} \end{bmatrix} \end{cases} \tag{9}$$

$$\mathbf{u} (k) = -\mathbf{K}_{LQR} \mathbf{x} (k) \tag{10}$$

Next, a discrete-time H_∞ controller is designed. As explained in the work of [32], H_∞ control is a game-theoretic approach to the disturbance attenuation problem. To design the discrete-time full-state feedback H_∞ controller for ARS, linear matrix inequality (LMI) is adopted. Under the full-state feedback control $\mathbf{u} = \mathbf{K}_\infty \mathbf{x}$, the system L_2 gain for the system (5) with (9) is said to be bounded or attenuated by χ if the condition (11) is satisfied.

$$\frac{\sum_{k=0}^{\infty} \mathbf{z}^T (k)\, \mathbf{z} (k)}{\sum_{k=0}^{\infty} \mathbf{w}^T (k)\, \mathbf{w} (k)} \leq \chi^2 \tag{11}$$

To find $\mathbf{K}_\infty$ which gives the minimum H_∞ norm χ, the following LMI is formulated [33]. From the solutions $\mathbf{P}$ and $\mathbf{Y}$ from LMI optimization (12), the H_∞ optimum controller gain matrix $\mathbf{K}_\infty$ is obtained as (13).

$$\begin{aligned} &\min_{\mathbf{P},\mathbf{Y},\chi} \ \chi \\ &\quad \mathbf{P} > 0, \ \chi > 0 \\ &s.t. \begin{bmatrix} -\mathbf{P} & \mathbf{\Phi P} + \mathbf{\Gamma}_u \mathbf{Y} & \mathbf{\Gamma}_w & \mathbf{0} \\ * & -\mathbf{P} & \mathbf{0} & (\mathbf{CP} + \mathbf{DY})^T \\ * & * & -\chi \mathbf{I} & \mathbf{0} \\ * & * & * & -\chi \mathbf{I} \end{bmatrix} < 0 \end{aligned} \tag{12}$$

$$\mathbf{u} (k) = \mathbf{K}_\infty \mathbf{x} (k) = \mathbf{Y}\mathbf{P}^{-1} \mathbf{x} (k) \tag{13}$$

Finally, a sliding mode controller is designed for ARS. The sliding or error surface is defined with the state vector $\mathbf{x}$ as shown in (14). To ensure that the sliding surface becomes zero, the convergence condition is defined as (15). The convergence condition (15) is very harsh that the controller designed by the condition can produce a very large control input [16]. As a result, roll responses of a vehicle with the controller show severe chattering phenomena. So, it is necessary to tune the convergence speed and the magnitude of the control input with a parameter. For the purpose, the modified convergence condition (16) is defined. In (16), α is a tuning parameter that regulates the convergence speed. Combining (5), (14), and (16) yields (17), and reorganizing this equation gives the control input $\mathbf{u}(k)$ as (18). In (18), $(\bullet)^+$ is a pseudo inverse of a matrix $\bullet$. As shown in (18), the control input $\mathbf{u}(k)$ consists of the feedback and feedforward terms.

$$\mathbf{s} (k) = \mathbf{H}\mathbf{x} (k) \tag{14}$$

$$\mathbf{s} (k+1) = \mathbf{s} (k) = 0 \tag{15}$$

$$\mathbf{s} (k+1) = \alpha \mathbf{s} (k) \quad (0 < \alpha < 1) \tag{16}$$

$$\begin{aligned} \mathbf{s} (k+1) &= \mathbf{H}\mathbf{\Phi}\mathbf{x} (k) + \mathbf{H}\mathbf{\Pi}\mathbf{w} (k) + \mathbf{H}\mathbf{\Gamma}\mathbf{u} (k) \\ &= \alpha \mathbf{H}\mathbf{x} (k) \end{aligned} \tag{17}$$

$$\begin{aligned} \mathbf{u} (k) &= -(\mathbf{H}\mathbf{\Gamma})^+ \mathbf{H} (\mathbf{\Phi} - \alpha \mathbf{I})\, \mathbf{x} (k) - (\mathbf{H}\mathbf{\Gamma})^+ \mathbf{H}\mathbf{\Pi}\mathbf{w} (k) \\ &= -\mathbf{K}_{SMC} \mathbf{x} (k) - \mathbf{K}_{SMCFF} \mathbf{w} (k) \end{aligned} \tag{18}$$

Finally, the feedforward controller is designed with the discrete-time state-space equation. It is assumed that a general type controller consists of a feedback controller $\mathbf{K}_{FB}$ and a feedforward one $\mathbf{K}_{FF}$, as shown in (19). Substituting (19) into (5) gives (20). As a condition for the state variable to be 0, all $\{\}$ terms in (20) should be set to 0. As a result, the gain matrices of feedback and feedforward controllers are obtained as (21). In (21), $\mathbf{K}_{FF}$ is used as a feedforward control, added to the previously derived LQR, H_∞ and SMC. $\mathbf{K}_{FF}$ is identical to that of (18), i.e., $(\mathbf{H}\Gamma)^+\mathbf{H}\Pi$ except the sign, and $\mathbf{K}_{FB}$ is identical to that of (18), i.e., $(\mathbf{H}\Gamma)^+\mathbf{H}\Phi$ except the sign if α is 0.

$$\mathbf{u} (k) = -\mathbf{K}_{FB} \mathbf{x} (k) - \mathbf{K}_{FF} \mathbf{w} (k) \tag{19}$$

$$\begin{aligned} \mathbf{x} (k+1) &= \mathbf{\Phi}\mathbf{x} (k) + \mathbf{\Pi}\mathbf{w} (k) + \mathbf{\Gamma}\mathbf{u} (k) \\ &= \mathbf{\Phi}\mathbf{x} (k) + \mathbf{\Pi}\mathbf{w} (k) + \mathbf{\Gamma} \{ -\mathbf{K}_{FB} \mathbf{x} (k) - \mathbf{K}_{FF} \mathbf{w} (k) \} \\ &= \{ \mathbf{\Phi} - \mathbf{\Gamma}\mathbf{K}_{FB} \} \mathbf{x} (k) + \{ \mathbf{\Pi} - \mathbf{\Gamma}\mathbf{K}_{FF} \} \mathbf{w} (k) \end{aligned} \tag{20}$$

$$\mathbf{K}_{FB} = \mathbf{\Gamma}^+ \mathbf{\Phi}, \quad \mathbf{K}_{FF} = \mathbf{\Gamma}^+ \mathbf{\Pi} \tag{21}$$

C. ACTUATORS FOR ARS

The control roll moment M_φ calculated in the controller is to be generated by an actuator in a real vehicle. For the purpose, an AARB and a CDC are adopted as an actuator in this article.

Fig. 4 shows the geometrical relationship between the force acting on suspensions F_{susp}, the control roll moment M_φ and the twisting moment M_T generated by an electric motor or hydraulic devices in AARB [1]. From the relationship given in Fig. 4, the force-moment relationship (22) is obtained. From (22), the required twisting moment M_T that an actuator should generate in AARB is simply calculated from M_φ, as given in (23). So, it is easy to apply the twisting moment of an actuator to generate M_φ with AARB.

$$F_{susp} = \frac{M_\phi}{L} = \frac{M_T}{b} \tag{22}$$

$$M_T = M_\phi \frac{b}{L} \tag{23}$$

Fig. 5 shows the characteristic curve of CDC [8]–[10]. The relationship between M_φ and the damping force, F_s,

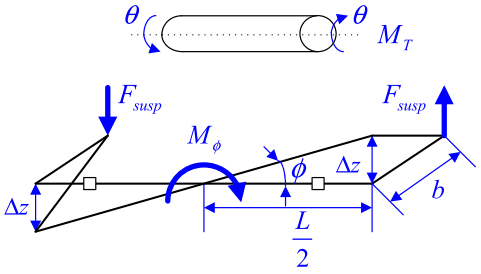

FIGURE 4. Geometrical relationship between the control roll moment and the force acting on the suspension.

is given by (24). In (24), ($\dot{z}_{sr}$-$\dot{z}_{ur}$) and ($\dot{z}_{sl}$-$\dot{z}_{ul}$) are the suspension stroke rates or suspension velocity of the right and left suspensions, respectively. Since CDC is a semi-active device, it can only prevent the compression and expansion of the suspension, and it cannot create active force. This fact is expressed by four conditions such as equations (25), (26), (27), and (28), and the value of the CDC current is determined accordingly [8-10]. In these equations, F_{sr} and F_{sl} are the forces of right and left suspensions, generated by the command currents, i_r and i_l, of CDC, respectively.

$$M_\phi = t\left[b_r\left(\dot{z}_{sr}-\dot{z}_{ur}\right)-b_l\left(\dot{z}_{sl}-\dot{z}_{ul}\right)\right] \tag{24}$$

i) $M_\phi\left(\dot{z}_{sr}-\dot{z}_{ur}\right)>0 \quad M_\phi\left(\dot{z}_{sl}-\dot{z}_{ul}\right)>0$

$$\Rightarrow \begin{cases} i_r = \begin{cases} 1, & if\ F_{sr} \geq F_{sr,\max} \\ \dfrac{F_{sr}-F_{sr,\min}}{F_{sr,\max}-F_{sr,\min}}, & \\ & if\ F_{sr} < F_{sr,\max}, \end{cases} \qquad i_l = 0 \end{cases} \tag{25}$$

ii) $M_\phi\left(\dot{z}_{sr}-\dot{z}_{ur}\right)>0, \quad M_\phi\left(\dot{z}_{sl}-\dot{z}_{ul}\right)<0$

$$\Rightarrow \begin{cases} i_r = \begin{cases} 1, & if\ F_{sr} \geq F_{sr,\max} \\ \dfrac{F_{sr}-F_{sr,\min}}{F_{sr,\max}-F_{sr,\min}}, & if\ F_{sr} < F_{sr,\max} \end{cases} \\ i_l = \begin{cases} 1, & if\ F_{sl} \geq F_{sl,\max} \\ \dfrac{F_{sl}-F_{sl,\min}}{F_{sl,\max}-F_{sl,\min}}, & if\ F_{sl} < F_{sl,\max} \end{cases} \end{cases} \tag{26}$$

iii) $M_\phi\left(\dot{z}_{sr}-\dot{z}_{ur}\right)<0, \quad qM_\phi\left(\dot{z}_{sl}-\dot{z}_{ul}\right)>0 \Rightarrow \begin{cases} i_r = 0 \\ i_l = 0 \end{cases}$ (27)

iv) $M_\phi\left(\dot{z}_{sr}-\dot{z}_{ur}\right)<0, \quad M_\phi\left(\dot{z}_{sl}-\dot{z}_{ul}\right)<0$

$$\Rightarrow \begin{cases} i_r = 0 \\ i_l = \begin{cases} 1, & if\ F_{sl} \geq F_{sl,\max} \\ \dfrac{F_{sl}-F_{sl,\min}}{F_{sl,\max}-F_{sl,\min}}, & if\ F_{sl} < F_{sl,\max} \end{cases} \end{cases} \tag{28}$$

III. DISTURBANCE OBSERVER DESIGN

As shown in (10), (13), (18) and (21) representing the controllers, the roll angle, roll rate, and lateral acceleration are required to calculate the control roll moment. In general, it is known that the roll angle of a vehicle is very difficult to measure. Instead, the roll rate can be measured relatively easily using a sensor that is currently available on the market [20], [21]. In this article, a DTKF is designed to estimate the roll angle and the lateral acceleration using the roll rate signal. In general, the lateral acceleration signal measured with a sensor installed on the vehicle is shown in Fig. 1. As shown in Fig. 1, it has a lot of noise. In order to use this signal for the controllers, it is necessary to filter the noises. For the purpose, a LPF has been used. However, if a LPF is used for noise filtering, a time delay occurs and control performance is deteriorated as a result. Therefore, in this article, a DTKF is applied to simultaneously estimate the roll angle, the state variable, and the lateral acceleration, the disturbance, using the measured roll rate signal.

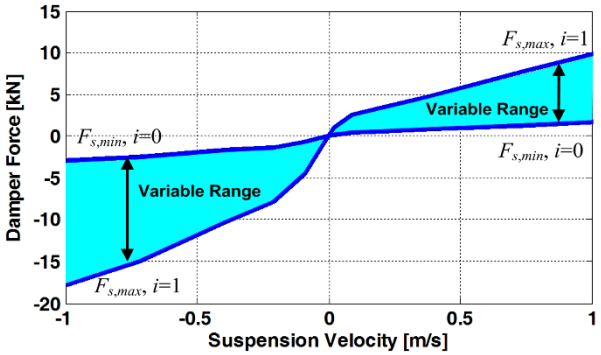

FIGURE 5. Characteristic curve of CDC.

For use in observers, the state variables and state vector are defined as (29) [19], [28]. The continuous-time state-space equation according to the vector of state variables is derived as (30) from (1) and (4). The matrices in (30) are defined in (31). If (30) is discretized by the sampling time T_s, it becomes (32). In (32), μ and ν are system and sensor noises, and the covariances of these signals are given by (33). As shown in the matrix $\mathbf{C}_e$ of (31), the sensor measurement used for the observer is the roll rate.

$$\mathbf{x}(t) = \left[\phi(t) \quad \dot{\phi}(t) \quad a_y(t)\right]^T \tag{29}$$

$$\begin{cases} \dot{\mathbf{x}}(t) = \mathbf{A}_e\mathbf{x}(t) + \mathbf{B}_e\mathbf{u}(t) + \boldsymbol{\mu}(t) \\ \mathbf{y}(t) = \mathbf{C}_e\mathbf{x}(t) + \boldsymbol{\nu}(t) \end{cases} \tag{30}$$

$$\begin{cases} \mathbf{A}_e = \begin{bmatrix} 0 & 1 & 0 \\ -\dfrac{K_\phi - m_s g h_s}{I_x} & -\dfrac{C_\phi}{I_x} & \dfrac{m_s h_s}{I_x} \\ 0 & 0 & 0 \end{bmatrix}, \\ \mathbf{B}_e = \begin{bmatrix} 0 \\ \dfrac{1}{I_x} \\ 0 \end{bmatrix} \\ \mathbf{C}_e = \begin{bmatrix} 0 & 1 & 0 \end{bmatrix} \end{cases} \tag{31}$$

$$\begin{cases} \mathbf{x}(k+1) = \mathbf{A}_d\mathbf{x}(k) + \mathbf{B}_d\mathbf{u}(k) + \boldsymbol{\mu}(k) \\ \mathbf{y}(k) = \mathbf{C}_d\mathbf{x}(k) + \boldsymbol{\nu}(k) \end{cases} \tag{32}$$

$$\mathbf{M}(k) = E\left\{\boldsymbol{\mu}(k)\boldsymbol{\mu}^T(k)\right\}, \quad \mathbf{N}(k) = E\left\{\boldsymbol{\nu}(k)\boldsymbol{\nu}^T(k)\right\} \tag{33}$$

In this article, the discrete-time Kalman filter (DTKF), given by (34) and (35), is used to estimate the roll angle and the lateral acceleration. Eqs. (34) and (35) of DTKF represent the prediction step using the state-space equation and the correction step using sensor measurements, respectively [34]. The controllers, (10), (13), (18) and (21), use the roll angle and lateral acceleration, estimated with the DTKF.

$$\begin{cases} \hat{\mathbf{x}}_{-}(k) = \mathbf{A}_d \hat{\mathbf{x}}(k-1) + \mathbf{B}_d \mathbf{u}(k-1) \\ \mathbf{P}_{-}(k) = \mathbf{A}_d \mathbf{P}(k-1) \mathbf{A}_d^T + \mathbf{M}(k) \end{cases} \tag{34}$$

$$\begin{cases} \mathbf{K}_e = \mathbf{P}_{-}(k) \mathbf{C}_d^T \left[\mathbf{C}_d \mathbf{P}_{-}(k) \mathbf{C}_d^T + \mathbf{N}(k) \right] \\ \hat{\mathbf{x}}(k) = \hat{\mathbf{x}}_{-}(k) + \mathbf{K}_e \left[\mathbf{y}(k) - \mathbf{C}_d \hat{\mathbf{x}}_{-}(k) \right] \\ \mathbf{P}(k) = (\mathbf{I} - \mathbf{K}_e \mathbf{C}_d) \mathbf{P}_{-}(k) \end{cases} \tag{35}$$

When running the DTKF, the parameters such as C_φ and K_φ in the 1-DOF roll model are assumed to be constant. However, these parameters are time-varying when a vehicle is driving. So, it is necessary to estimate the parameters with adaptation algorithms. In this article, RLS is adopted to do it. The vectors of parameters and state variables of RLS are defined in (36). In (36), T_φ is defined as K_φ-$m_s \cdot g \cdot h_s$. With the definitions and the equation of motion, (1), the output and the error are defined as (37) and (38), respectively. The update equations of RLS are given by (39).

$$\begin{aligned} &\theta(k) \\ &= \begin{bmatrix} T_\phi & C_\phi \end{bmatrix}^T, \quad \varphi(k) = \begin{bmatrix} \hat{\phi}(k) & \dot{\hat{\phi}}(k) \end{bmatrix}^T \end{aligned} \tag{36}$$

$$\begin{aligned} &y(k) \\ &= \varphi^T(k)\theta(k) + e(k) \\ &= M_\phi - I_x \ddot{\phi} + m_s h_s a_y \end{aligned} \tag{37}$$

$$\begin{aligned} &e(k+1) \\ &= y(k) - \varphi^T(k+1)\hat{\theta}(k) \end{aligned} \tag{38}$$

$$\begin{cases} \mathbf{K}(k+1) = \mathbf{P}(k+1)\varphi(k+1) \\ \qquad = \dfrac{\mathbf{P}(k)\varphi(k+1)}{1 + \varphi^T(k+1)\mathbf{P}(k)\varphi(k+1)} \\ \hat{\theta}(k+1) = \hat{\theta}(k) + \mathbf{K}(k+1)e(k+1) \\ \mathbf{P}(k+1) \\ \qquad = \mathbf{P}(k)\left[\mathbf{I} - \dfrac{\varphi(k+1)\varphi^T(k+1)\mathbf{P}(k)}{1 + \varphi^T(k+1)\mathbf{P}(k)\varphi(k+1)} \right] \end{cases} \tag{39}$$

The parameter estimation with RLS is combined with the DTKF, as defined above. For the given parameters, T_φ and C_φ, the state variables are estimated with DTKF. With the estimated state variables, the parameters, T_φ and C_φ, are updated with RLS [25]. Then, these estimated values are used to update $\mathbf{A}_d$ and $\mathbf{B}_d$ in (34), and these matrices are used in DTKF.

IV. SIMULATION

Simulation was performed on the vehicle simulation package CarSim to verify the effectiveness of the feedforward controller and the disturbance observer. The simulation condition is to follow a moose driving track using the driver model provided by CarSim [35]. The preview time of the driver model is 0.75 seconds compared to the vehicle speed, indicating an inexperienced driver. The target vehicle is a small-sized SUV provided by CarSim. This model is 27-DOF nonlinear one with a single sprung mass, four wheels, suspensions and a steering mechanism. The suspensions of the model consist of front independent and rear solid axles. A spring and a damper in this model are nonlinear ones fitted by piece-wise linear interpolation [35]. The parameters of the model needed to design the controllers are given in Table 1. The initial vehicle speed and the tire-road friction coefficient were set to 80km/h and 0.6, respectively. The simulation period is 10 seconds. The sampling time T_s of the controllers is set to 10ms.

TABLE 1. Parameters of the small-sized SUV model.

m_s	984 kg	I_x	442 kg·m^2
C_ϕ	7,600 N·m·s/rad	K_ϕ	64,800 N·m/rad
h_s	0.45 m		

TABLE 2. Weights in LQ objective function and covariances of noises for Kalman filter.

ρ_1	1 deg	ρ_1	10 deg/s
ρ_1	2000 N·m	$\mathbf{H}$	$\begin{bmatrix} 10 & 1 \end{bmatrix}$
$\mathbf{M}$	$\begin{bmatrix} 1e-4 & 0 & 0 \\ 0 & 1e0 & 0 \\ 0 & 0 & 1e3 \end{bmatrix}$	$\mathbf{N}$	1e-2

In the SMC, the value of α was set to 0.5. The weight of the LQ objective function and the covariance matrices of the noises used in the DTKF are set as shown in Table 2. In Table 2, the maximum allowable values of the roll angle and the roll rate, i.e., ρ_1 and ρ_2, are set to 1deg and 10deg/s, respectively. Following the weights, the matrix $\mathbf{H}$ of SMC was set to [10 1] in Table 2. The gain matrix of the feedforward controller is $\mathbf{K}_{FF}$ in (21). The gain matrices of LQR, H_∞ controller and SMC are given in (40). With these matrices, all the closed-loop systems are stable because all the poles of the systems reside within a unit-circle. AARB and CDC were used as the actuator for the roll motion control. These are modeled as a first-order system whose the time constants were set to 0.01 and 0.1, respectively.

$$\begin{cases} \mathbf{K}_{LQR} = \begin{bmatrix} 38315 & 4232 \end{bmatrix} \\ \mathbf{K}_{\infty} = \begin{bmatrix} 113700 & 18860 \end{bmatrix} \\ \mathbf{K}_{SMC} = \begin{bmatrix} 90670 & 9981 \end{bmatrix} \end{cases} \tag{40}$$

In general, when the roll motion of the vehicle is controlled, the control performance for the yaw motion is deteriorated due to the lateral load transfer. To prevent this, a yaw moment controller should be applied. In this article, the previously proposed Unified Chassis Control (UCC) is applied [36]. The UCC uses Electronic Stability Control (ESC) and Active

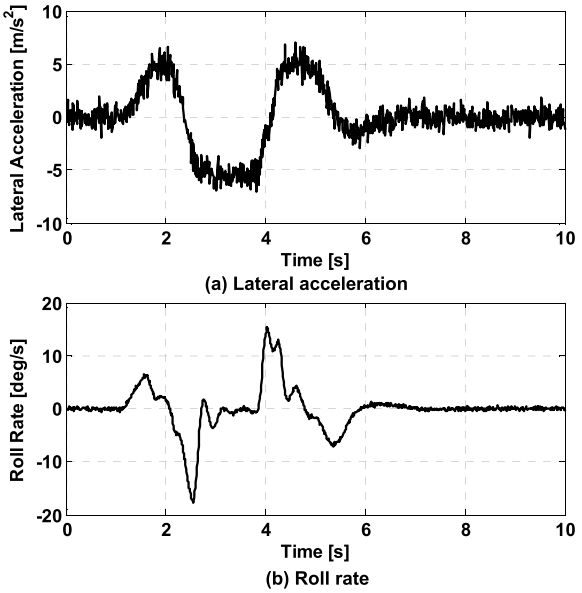

FIGURE 6. Lateral acceleration signal from on-board accelerometer.

Front Steering (AFS) as an actuator to generate a control yaw moment. In this article, the ratio of use of ESC and AFS in UCC was set at 50%:50%.

Fig. 6 shows the lateral acceleration and roll rate signals directly obtained from simulation in CarSim. White noises with different variances were added to those signals. As shown in Fig. 6, the roll rate signal has a small amount of noises, but the lateral acceleration does a large amount of ones. Hereafter in the simulation, the white noises with identical variances are always added to the lateral acceleration and the roll rate signals.

In simulation, three cases are considered according to the use of signals. The first case, CASE1, means that the roll angle and the lateral acceleration signals are obtained directly from CarSim, and fed to the controllers. There are no observers for CASE1. So, the noises in those signals directly passed into the control input. The second case, CASE2, means that the roll angle and the lateral acceleration are estimated using DTKF with the measured roll rate signal. The third case, CASE3, is identical to CASE2 except that DTKF is replaced with DTKF+RLS.

The first simulation is done with AARB for three cases. The control roll moment is divided by 2, and applied to front and rear AARBs. Each AARB has the limit torque of 2000N·m. Figs. 7 and 8 show the simulation results for each controller with feedback, and feedback and feedforward, respectively. In Fig. 8, the legend DFF means the disturbance feedforward with the lateral acceleration signal. As shown in these figures, the controllers with the feedforward controller show better performance than those with only feedback one. This is achieved by virtue of the feedforward control with the lateral acceleration. However, as shown in Fig. 8-(c), the control roll moment has a large amount of noises passed from the lateral acceleration signal. So, the roll rate responses of

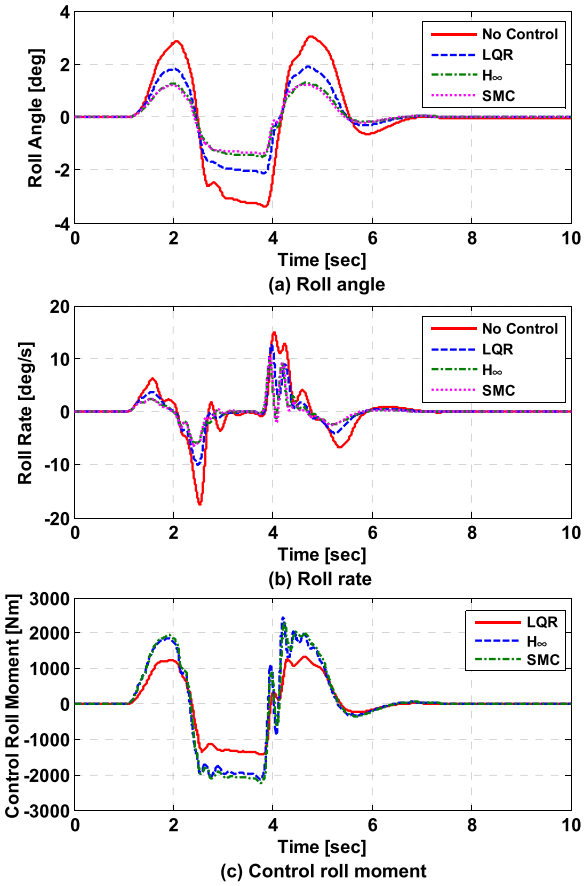

FIGURE 7. Simulation results of each controller with feedback for CASE1.

these controllers show chattering after those converge to 0, as shown in Fig. 8-(b).

Figs. 9 and 10 show the simulation results for CASE2 and CASE3. In these cases, the roll angle and the lateral acceleration were estimated from the roll rate signal with DTKF or DTKF+RLS. As shown in these figures, the results are nearly identical to those given in Figs. 7 and 8, except the control roll moment. During the estimation with DTKF or DTKF+RLS, the noises in the roll rate signals are filtered. So, the control roll moment from the feedforward controller was smoothed by the filtering effect of DTKF or DTKF+RLS, as shown in Figs. 9-(c) and 10-(c). Compared to the results given in Fig. 8-(b), the chattering of the roll rate response after convergence to zero is reduced by the smoothed control roll moment. In Figs. 9-(e) and 10-(e), the estimation errors of the lateral acceleration are noisy because the original one used for comparison is noisy. The estimation results of DTKF and DTKF+RLS are nearly identical. So, it can be concluded that RLS has little effect on the estimation performance for ARS.

Table 3 and 4 show the several performance measures of the controllers for CASE2 and CASE3. As shown in these tables, the feedforward controller significantly improves the control performance, compared to the feedback only case. The estimation errors for the roll angle and the lateral acceleration are so small that it can be used for control purpose.

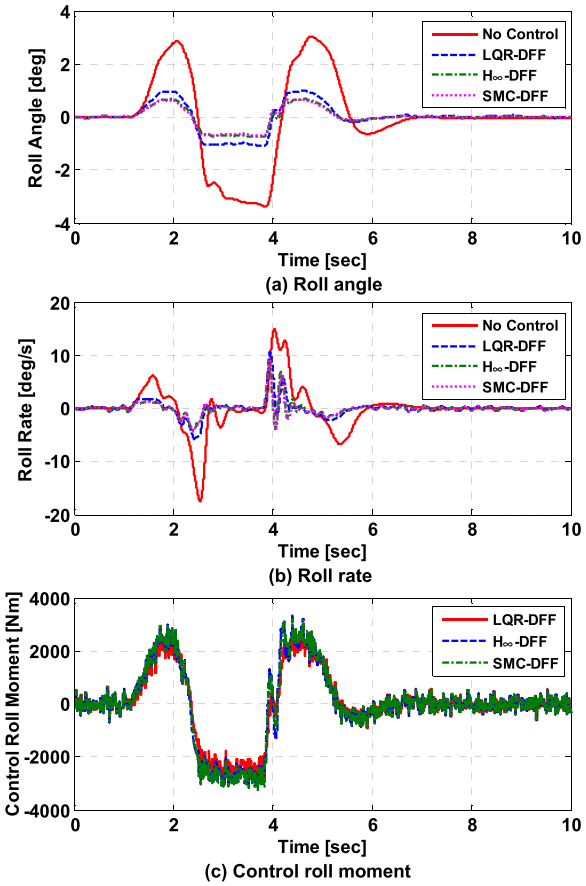

FIGURE 8. Simulation results of each controller with feedback and feedforward for CASE1.

TABLE 3. Summary of performance measures for CASE2 with AARB.

	Max. $\lvert\phi\rvert$ (deg)	Max. $\lvert\dot{\phi}\rvert$ (deg/s)	Max. $\lvert M_\phi\rvert$ (Nm)	Max. $\lvert\phi_{error}\rvert$ (deg)	Max. $\lvert a_{yerror}\rvert$ (m/s^2)
No Control	3.4	17.5			
LQR	2.1	12.6	1402	0.10	
H_∞	1.5	9.5	2465	0.13	
SMC	1.4	10.2	2329	0.13	
LQR-DFF	1.2	11.0	2469	0.13	1.5
H_∞-DFF	0.8	8.5	2859	0.13	1.3
SMC-DFF	0.8	9.2	2872	0.13	1.2

As mentioned earlier, the difference between DTKF and DTKF+RLS is quite small. The only difference is that RLS slightly improves the estimation on the lateral acceleration. So, it can be also concluded that RLS has little effect on the estimation performance of DTKF.

The second simulation is done with CDC for three cases. CDC is a semi-active type actuator, which cannot generate a fully active force. So, the control performance with CDC is deteriorated, compared to the active one, i.e., AARB. The characteristic curve of CDC in Fig. 5 is used by multiplying 3 to it. Figs. 11 and 12 show the simulation results of CASE1 and CASE2. By comparing Figs. 11-(c) with 12-(c),

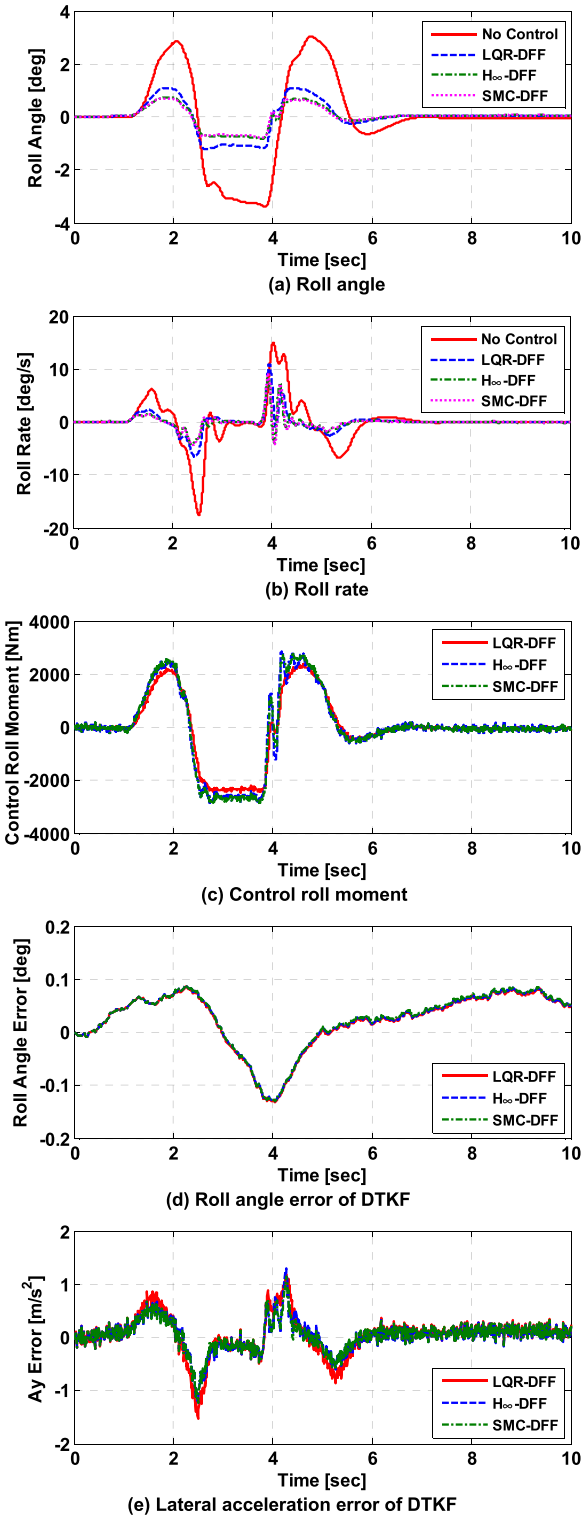

FIGURE 9. Simulation results of each controller with disturbance feedforward for CASE2.

DTKF has the filtering effect on the noises in the measured roll rate signals. As shown in these figures, three controllers show nearly identical performance although the control roll moments of the controllers are different. This is caused by

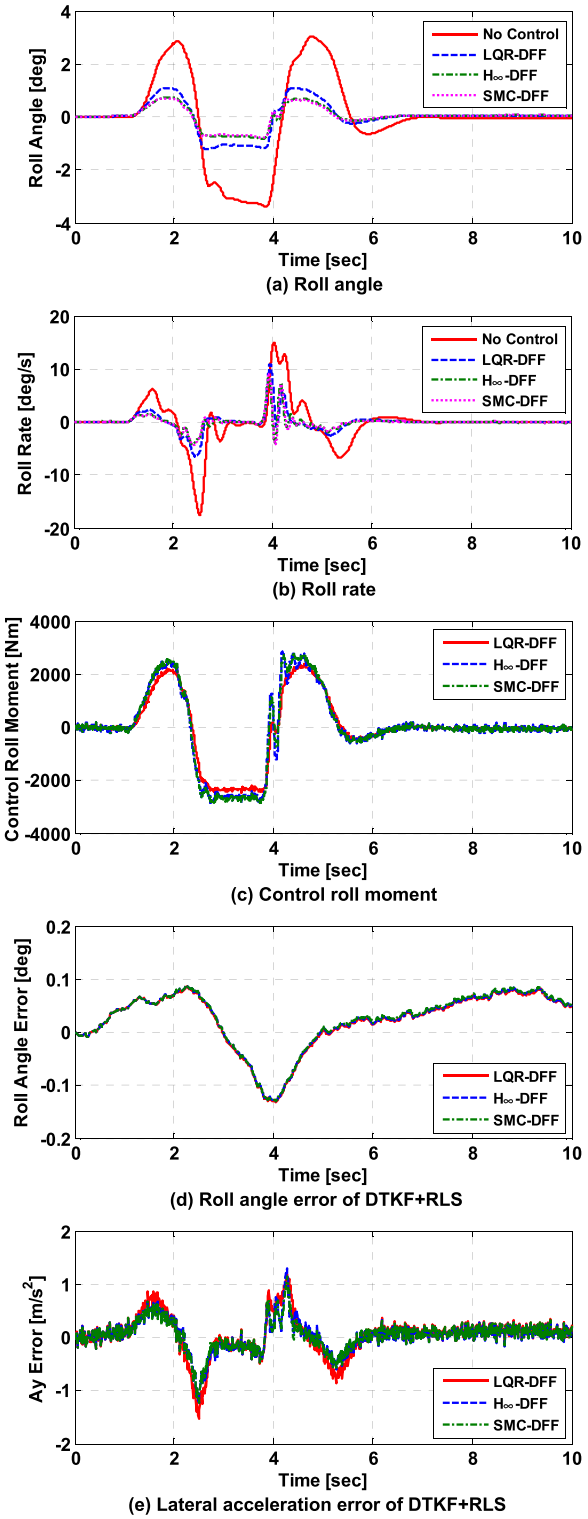

FIGURE 10. Simulation results of each controller with disturbance feedforward for CASE3.

the fact that the force generated by CDC is limited. In other words, the control roll moment and the moment generated by CDC force are different. The latter is smaller than the former. This is the typical actuator saturation or actuator nonlinearity.

TABLE 4. Summary of performance measures for CASE3 with AARB.

	Max. $\lvert\phi\rvert$ (deg)	Max. $\lvert\dot{\phi}\rvert$ (deg/s)	Max. $\lvert M_\phi\rvert$ (Nm)	Max. $\lvert\phi_{error}\rvert$ (deg)	Max. $\lvert a_{y,error}\rvert$ (m/s^2)
No Control	3.4	17.5			
LQR	2.1	12.6	1402	0.10	
H_∞	1.5	9.5	2465	0.13	
SMC	1.4	10.2	2329	0.13	
LQR-DFF	1.2	11.0	2469	0.13	1.5
H_∞-DFF	0.8	8.5	2859	0.13	1.2
SMC-DFF	0.8	9.2	2872	0.13	1.2

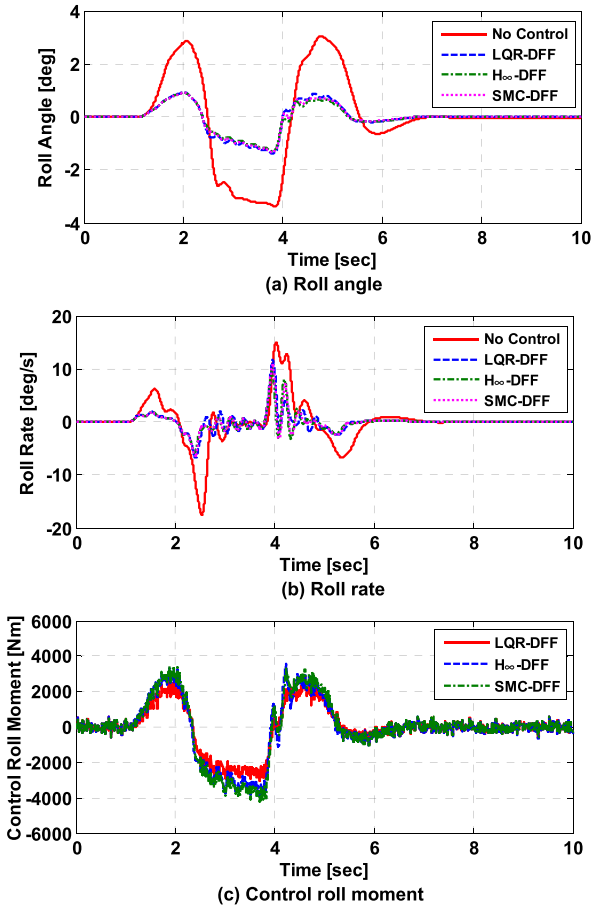

FIGURE 11. Simulation results of each controller with feedback and disturbance feedforward for CASE1.

This fact can be checked from Fig. 13 that CDC forces of the feedback and the feedforward controller are nearly identical. This can cause the deterioration of the estimation performance of DTKF. As shown in Fig. 12-(d) and -(e), the estimation results are worse than those of AARB because CDC cannot fully generate the given control roll moment. Especially, the estimation performance on the lateral acceleration become worse. To cope with this problem, a nonlinear observer is needed, which can handle the actuator saturation or nonlinearity [37].

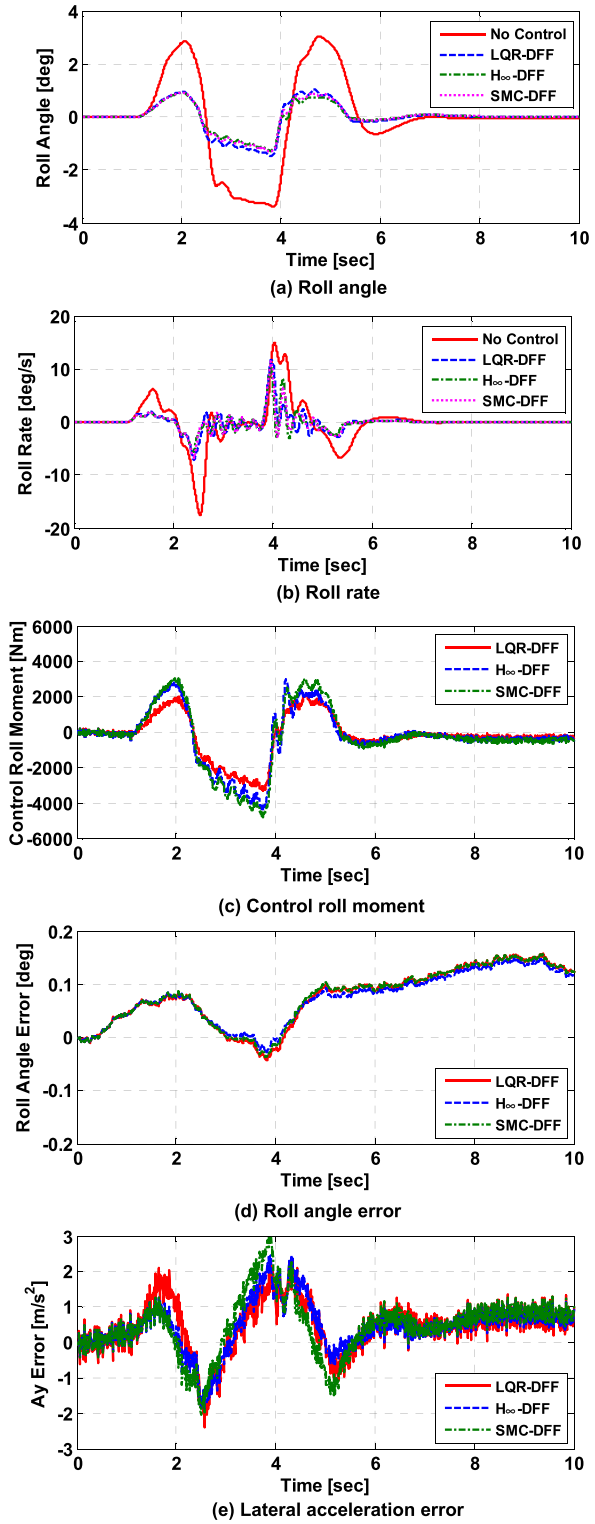

FIGURE 12. Simulation results of each controller with feedback and disturbance feedforward for CASE2.

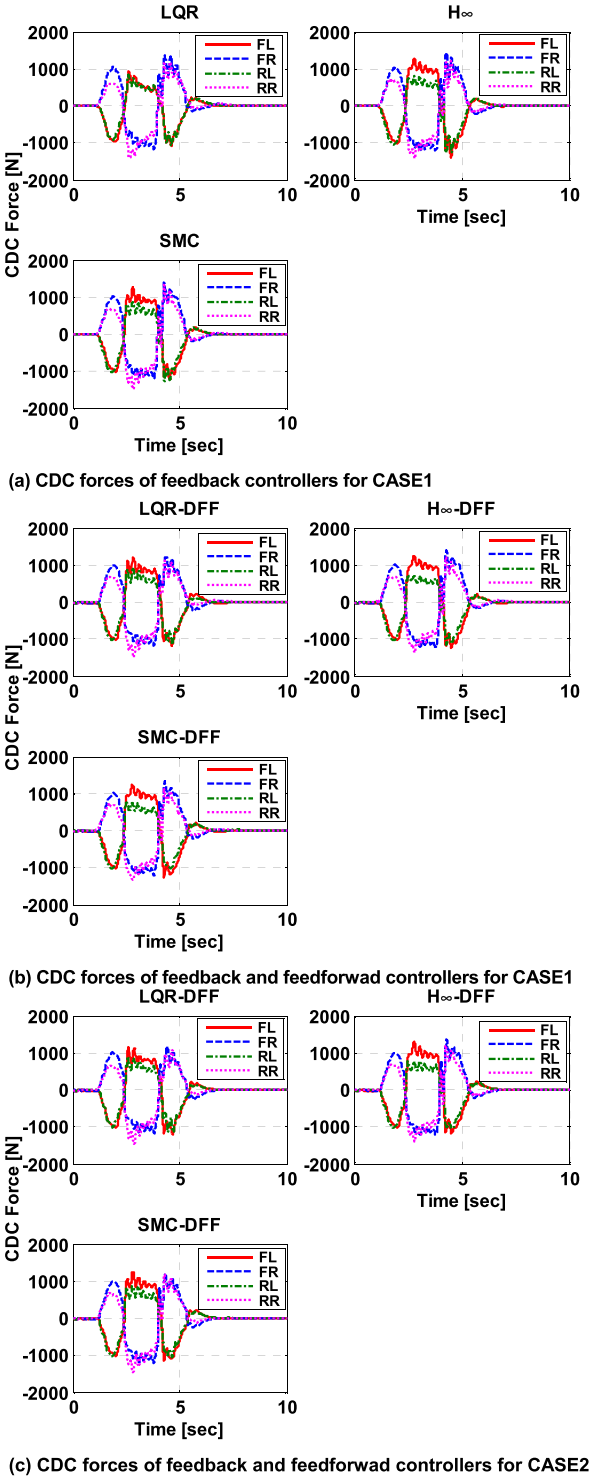

FIGURE 13. CDC forces of each controller for CASE1 and CASE2.

Table 5 and 6 summarize the simulation results of the controllers with CDC for CASE2 and CASE3. As shown in these tables, H_∞ and SMC show the nearly identical performance for ARS. In other words, the feedforward controller did not improve the control performance except LQR. This is caused by the saturation effect of CDC, compared to AARB. Due to the actuator saturation of CDC, the feedforward controller has little effect on ARS. For the reason, the estimation performances of DTKF and DTKF+RLS worse than those given in Table 3 and 4. Notable feature from Table 5 and 6 is that the

TABLE 5. Summary of performance measures for CASE2 with CDC.

	Max. $\lvert\phi\rvert$ (deg)	Max. $\lvert\dot{\phi}\rvert$ (deg/s)	Max. $\lvert M_\phi\rvert$ (Nm)	Max. $\lvert\phi_{error}\rvert$ (deg)	Max. $\lvert a_{y,error}\rvert$ (m/s^2)
No Control	3.4	17.5			
LQR	1.6	10.9	1102	0.13	
H_∞	1.2	9.1	2165	0.15	
SMC	1.3	10.1	2192	0.14	
LQR-DFF	1.5	11.7	3311	0.16	2.4
H_∞-DFF	1.3	10.4	4377	0.15	2.5
SMC-DFF	1.3	11.2	4771	0.16	3.3

TABLE 6. Summary of performance measures for CASE3 with CDC.

	Max. $\lvert\phi\rvert$ (deg)	Max. $\lvert\dot{\phi}\rvert$ (deg/s)	Max. $\lvert M_\phi\rvert$ (Nm)	Max. $\lvert\phi_{error}\rvert$ (deg)	Max. $\lvert a_{y,error}\rvert$ (m/s^2)
No Control	3.4	17.5			
LQR	1.6	10.9	1103	0.14	
H_∞	1.2	9.2	2110	0.16	
SMC	1.3	10.1	2198	0.15	
LQR-DFF	1.4	11.7	3164	0.16	2.3
H_∞-DFF	1.3	10.8	4237	0.16	2.5
SMC-DFF	1.3	11.6	4626	0.16	3.3

performances of the feedback controllers with CDC are better than those of AARB. This is caused by the nonlinear effect of CDC, as given in Fig. 5.

V. CONCLUSION

In this article, three feedback controllers, LQR, H_∞ and SMC, were designed with 1-DOF roll model for ARS. For performance improvement, the feedforward controller with the lateral acceleration was designed from the discrete-time state-space model. To estimate the roll angle and the lateral acceleration simultaneously, DTKF was designed with measured roll rate signal. With the DTKF, the noise in the roll rate signal can be filtered. So, a LPF was not needed to filter the noises in the roll rate and lateral acceleration signals. For parameter estimation in DTKF, RLS was applied to DTKF. As an actuator for ARS, AARB and CDC were adopted. Through simulation in CarSim, it was shown that the feedforward controller with the estimated lateral acceleration can significantly improve the control performance for ARS if AARB is used as an actuator. RLS was shown to have little effect on the estimation performance. With CDC for ARS, it was checked that the performance improvement is limited to a certain level because of the saturation effect of CDC. As a result, the feedforward controller has little effect on the control performance when using CDC. It was also shown that the feedback controllers with CDC can give better control performance than those with AARB. To cope with these problems caused by CDC, it is necessary to apply a nonlinear observer which can handle the actuator saturation or nonlinearity [37].

REFERENCES

[1] A. Sorniotti, A. Morgando, and M. Velardocchia, "Active roll control: System design and hardware-in-the-loop test bench," *Vehicle Syst. Dyn.*, vol. 44, pp. 489–505, Apr. 2006.
[2] Y. Mizuta, M. Suzumura, and S. Matsumoto, "Ride comfort enhancement and energy efficiency using electric active stabiliser system," *Vehicle Syst. Dyn.*, vol. 48, no. 11, pp. 1305–1323, Nov. 2010.
[3] M. Takahashi, T. Kumamaru, and K. Yoshida, "Integrated controller design for automotive semi-active suspension considering vehicle behavior with steering input," in *New Trends and Developments in Automotive System Engineering*, M. Chiaberge, Ed. Rijeka, Croatia: InTechOpen, 2011, doi: 10.5772/14287.
[4] Y. Ohta, H. Kato, D. Yamada, K. Sato, T. Fukino, E. Nobuyama, and S. Buma, "Development of an electric active stabilizer, system based on robust design," SAE Tech. Papers 2006-01-0758, 2006.
[5] M. Straßberger and J. Guldner, "BMW's dynamic drive: An active stabilizer bar system," *IEEE Control Syst. Mag.*, vol. 24, no. 4, pp. 28–29, Aug. 2004.
[6] G. Koch, O. Fritsch, and B. Lohmann, "Potential of low bandwidth active suspension control with continuously variable damper," *Control Eng. Pract.*, vol. 18, no. 11, pp. 1251–1262, Nov. 2010.
[7] J. H. Crews, M. G. Mattson, and G. D. Buckner, "Multi-objective control optimization for semi-active vehicle suspensions," *J. Sound Vib.*, vol. 330, no. 23, pp. 5502–5516, Nov. 2011.
[8] W. Cho, J. Yoon, J. Kim, J. Hur, and K. Yi, "An investigation into unified chassis control scheme for optimised vehicle stability and manoeuvrability," *Vehicle Syst. Dyn.*, vol. 46, no. 1, pp. 87–105, 2008.
[9] J. Yoon, S. Yim, W. Cho, B. Koo, and K. Yi, "Design of an unified chassis controller for rollover prevention, manoeuvrability and lateral stability," *Vehicle Syst. Dyn.*, vol. 48, no. 11, pp. 1247–1268, Nov. 2010.
[10] S. Yim, N. Kim, S. W. Hwang, and S. H. Lee, "Preview controller design for active roll control with V2 V communication and continuous damping control," *J. Inst. Control, Robot. Syst.*, vol. 23, no. 12, pp. 1020–1026, Dec. 2017.
[11] H.-J. Kim and Y.-P. Park, "Investigation of robust roll motion control considering varying speed and actuator dynamics," *Mechatronics*, vol. 14, no. 1, pp. 35–54, Feb. 2004.
[12] D. J. M. Sampson and D. Cebon, "Active roll control of single unit heavy road vehicles," *Vehicle Syst. Dyn.*, vol. 40, no. 4, pp. 229–270, Oct. 2003.
[13] K. Jeon, H. Hwang, S. Choi, J. Kim, K. Jang, and K. Yi, "Development of an electric active rollcontrol (ARC) algorithm for a SUV," *Int. J. Automot. Technol.*, vol. 13, no. 2, pp. 247–253, 2012.
[14] S. Yim, K. Jeon, and K. Yi, "An investigation into vehicle rollover prevention by coordinated control of active anti-roll bar and electronic stability program," *Int. J. Control, Autom. Syst.*, vol. 10, no. 2, pp. 275–287, Apr. 2012.
[15] S. Yim and K. Yi, "Design of an active roll control system for hybrid four-wheel-drive vehicles," *Proc. Inst. Mech. Eng., D, J. Automobile Eng.*, vol. 227, no. 2, pp. 151–163, Feb. 2013.
[16] S. Yim, "Design of preview controllers for active roll stabilization," *J. Mech. Sci. Technol.*, vol. 32, no. 4, pp. 1805–1813, 2018.
[17] S. Yim, "Active roll preview control with V2 V communication," *Int. J. Automot. Technol.*, vol. 20, no. 1, pp. 169–175, Feb. 2019.
[18] J. Nah and S. Yim, "Observer-based active roll preview control with V2 V communication," *IEEE Access*, vol. 7, pp. 44831–44839, 2019.
[19] J. Nah and S. Yim, "Design of feedforward controller for active roll stabilization," *J. Inst. Control, Robot. Syst.*, vol. 25, no. 6, pp. 578–584, Jun. 2019.
[20] B. Motorsport. (2018). *Acceleration Sensor MM5.10-R.* [Online]. Available: http:// www.bosch-motorsport.de/content/downloads/Products /16727677195.html
[21] H. Aerospace. *HG1120 MEMS Inertial Measurement Unit.* Accessed: 2018. [Online]. Available: https://aerospace.honeywell.com/ en/~/media/aerospace/ files/brochures/n61-1524-000-004-hg1120-mems-inertial-measurement-unit-bro.pdf
[22] Oxford Technical Solutions. *RT3000 Inertial and GPS Measurement System: User Manual.* Accessed: 2019. [Online]. Available: https://www.oxts.com/wp-content/uploads/2020/03/rtman-200302.pdf
[23] J. Oh and S. B. Choi, "Vehicle roll and pitch angle estimation using a cost-effective six-dimensional inertial measurement unit," *Proc. Inst. Mech. Eng., D, J. Automobile Eng.*, vol. 227, no. 4, pp. 577–590, Apr. 2013.

[24] J. Garcia Guzman, L. Prieto Gonzalez, J. Pajares Redondo, S. Sanz Sanchez, and B. Boada, "Design of low-cost vehicle roll angle estimator based on Kalman filters and an IoT architecture," *Sensors*, vol. 18, no. 6, p. 1800, Jun. 2018.
[25] M. Park and S. Yim, "Design of robust observers for active roll control," *IEEE Access*, vol. 7, pp. 173034–173043, 2019.
[26] A. Radke and Z. Gao, "A survey of state and disturbance observers for practitioners," in *Proc. Amer. Control Conf.*, 2006, pp. 5183–5188.
[27] P. Yih, "Steer-by-wire: Implications for vehicle handling and safety," Ph.D. dissertation, Stanford Univ., Stanford, CA, USA, 2005.
[28] R. Rajamani, D. Piyabongkarn, V. Tsourapas, and J. Y. Lew, "Parameter and state estimation in vehicle roll dynamics," *IEEE Trans. Intell. Transp. Syst.*, vol. 12, no. 4, pp. 1558–1567, Dec. 2011.
[29] R. Tafner, M. Reichhartinger, and M. Horn, "Robust vehicle roll dynamics identification based on roll rate measurements," in *Proc. Workshop Engine Powertrain Control, Simulation Modeling (IFAC)*, Paris, France, 2012, pp. 72–78.
[30] K. Nam, S. Oh, H. Fujimoto, and Y. Hori, "Estimation of sideslip and roll angles of electric vehicles using lateral tire force sensors through RLS and Kalman filter approaches," *IEEE Trans. Ind. Electron.*, vol. 60, no. 3, pp. 988–1000, Mar. 2013.
[31] K. Jiang, A. C. Victorino, and A. Charara, "Adaptive estimation of vehicle dynamics through RLS and Kalman filter approaches," in *Proc. IEEE 18th Int. Conf. Intell. Transp. Syst.*, Sep. 2015, pp. 1741–1746.
[32] J. C. Doyle, K. Glover, P. P. Khargonekar, and B. A. Francis, "State-space solutions to standard H_2 and H_∞ control problems," *IEEE Trans. Autom. Control*, vol. 34, no. 8, pp. 831–847, Aug. 1989.
[33] M. C. de Oliveira, J. C. Geromel, and J. Bernussou, "An LMI optimization approach to multiobjective controller design for discrete-time systems," in *Proc. 38th IEEE Conf. Decis. Control*, Phoenix, Arizona, USA, Dec. 1999, pp. 3611–3616.
[34] D. Simon, *Optimal State Estimation: Kalman, H_∞ and Nonlinear Approaches*. Hoboken, NJ, USA: Wiley, 2006.
[35] *Mechanical Simulation Corporation, VS Browser: Reference Manual*, The graphical user interfaces of BikeSim, CarSim, and TruckSim, Ann Arbor, MI, USA, 2009.
[36] S. J. Yim, "Unified chassis control with electronic stability control and active front steering for under-steer prevention," *Int. J. Automot. Technol.*, vol. 16, no. 5, pp. 775–782, Oct. 2015.
[37] S. Ding, W. Chen, K. Mei, and D. J. Murray-Smith, "Disturbance observer design for nonlinear systems represented by input–output models," *IEEE Trans. Ind. Electron.*, vol. 67, no. 2, pp. 1222–1232, Feb. 2020.

SEONGJIN YIM (Member, IEEE) received the B.S. degree in mechanical engineering from Yonsei University, South Korea, in 1995, and the M.S. and Ph.D. degrees in mechanical engineering from the Korea Advanced Institute of Science and Technology (KAIST), in 1997 and 2007, respectively.

From 2008 to 2010, he was a Postdoctoral Researcher with the BK21 School for Creative Engineering Design of Next Generation Mechanical and Aerospace Systems, Seoul National University. From 2011 to 2013, he was a Research Professor with the Advanced Institutes of Convergence Technology, Seoul National University. Since 2019, he has been an Associate Professor with the Department of Mechanical and Automotive Engineering, Seoul National University of Science and Technology, South Korea. His research interests include integrated chassis control systems with V2V communication, active roll control with state and parameter estimation, electric power steering, and steer-by-wire systems.